Small-Angle Light Scattering from Nematic Liquid Crystals: Fluctuations of Director Field Due to Many-Body Interactions of Disclinations

T. Hashimoto,* A. Nakai, T. Shiwaku, and H. Hasegawa

Department of Polymer Chemistry, Kyoto University, Kyoto 606, Japan

S. Rojstaczer and R. S. Stein

Polymer Research Institute, University of Massachusetts, Amherst, Massachusetts 01003.
Received December 28, 1987; Revised Manuscript Received June 8, 1988

ABSTRACT: Small-angle light-scattering patterns from nematic liquid crystals were investigated on two kinds of semiflexible polyesters with mesogenic groups and flexible spacers in the main chains which can form thermotropic liquid crystals. Unique polarized and depolarized scattering patterns with a maximum intensity at a particular scattering angle θ_{max} ($\neq 0°$) and azimuthal angle μ_{max} were observed, μ_{max} being at odd multiples of 45° for V_v and at integer multiples of 90° for H_v patterns. The patterns were analyzed in terms of a proposed scattering theory developed for a model for an isolated disk having disclination lines of various strengths and signs at its center. Comparisons of the observed and calculated patterns suggest that the isolated model poorly describes the observed scattering and that the scattering arises primarily from the collection of disclinations, i.e., from fluctuations of the director field caused by many-body interactions of the disclinations, and reflects a spatial distribution in orientation and position of the disclinations.

I. Introduction

The Schlieren texture found in nematic liquid crystals is believed to result from orientation fluctuations of the director field $\mathbf{n}(\mathbf{r})$ caused by a spatial distribution of the disclinations (position and orientation) and by many-body interactions of the disclinations, i.e., discontinuous points or lines in the director field.[1,2] The disclinations cause the distortion of the director field, which gives an excess free energy of the nematic liquid crystals. The distortions of the director field and the free energy associated with them may be described in terms of three kinds of principal deformations, i.e., splay, twist, and bend with their corresponding elastic constants.[2]

In this paper we will investigate the spatial correlation of the fluctuations of the director field in thermotropic polymer liquid crystals by depolarized (H_v) and polarized components (V_v) of the small-angle light scattering. The Schlieren texture and corresponding unique scattering patterns will be presented in section II. The observed scattering patterns will be compared with the theoretical patterns calculated for the simplest possible model, i.e. an isolated circular disk with radius R which contains a single disclination of a given strength and sign at the center and the relevant director field $\mathbf{n}(\mathbf{r})$ as its internal structure (section III). The calculated patterns will be compared with the observed patterns (section III-4), the results of which indicated that the model is an oversimplification of the real structure. The observed scattering patterns are proposed to arise from many-body interactions of the disclinations which will cause fluctuations of the director field (section IV).

II. Experimental Section

II-1. Specimens and Methods. Two kinds of polyesters that form thermotropic liquid crystals were used in these studies. One type of material is poly[(ethylene terephthalate)-*co*-(*p*-oxybenzoate)] with 60 mol % *p*-oxybenzoate (POB) units (X-7G, Tennessee Eastman Co.) which is known as a main-chain thermotropic liquid crystalline polymer.[3] The other material is an aromatic polyester based on a triad ester mesogenic unit containing an arylsulfonyl-substituted hydroquinone, its synthesis and characterization being described elsewhere.[4] This polymer has a glass transition temperature T_g = 87 °C, a crystal to nematic transition T_{c-n} = 100 °C, and a nematic to isotropic transition T_{n-i} = 170 °C.

Solvent-cast thin films of X-7G of ca. 1-μm thickness were prepared on microscope cover glasses by the same technique as described previously.[5] The as-cast films were transparent, optically isotropic, and homogeneous under the observation of an optical microscope.[6] Formation and time-evolution of Schlieren texture in the nematic liquid crystals were observed during the isothermal heat treatment of the thin films. For this purpose the thin as-cast films were placed on a heating stage (TH-600 Type, Linkam Scientific Co.) controlled at a preset temperature. The structure evolution after the temperature jump was observed in situ and in real time under a Nikon Optiphot-Pol XTP-11 polarizing microscope equipped with a TV camera, VTR, monitor, video-frame memory, and image digitizer.[6]

The semiflexible aromatic polyester films were cast from a THF solution, followed by heat treatment at a temperature above T_{n-i}, cooled down to a temperature between T_{c-n} and T_{n-i}, held at constant temperature for 5 min, and subsequently quenched to room temperature.

II-2. The Nematic Schlieren Texture. Figure 1 shows a typical nematic Schlieren texture observed under crossed Nicols (a), the spatial distribution of disclinations observed only with the polarizer (the analyzer being taken out) (b), and the strength and sign of the disclinations (c). Micrographs a and b were taken respectively 90 and 82 s after the temperature jump of the as-cast film of the X-7G to 240 °C. There is a slight time difference between micrographs a and b, because micrograph b was first taken with only the polarizer, then the sign and strength of the Schlieren texture were investigated by inserting the analyzer and by rotating the polarizer and analyzer maintaining the crossed position, and finally micrograph a was taken. Micrographs a–c were obtained for the same field.

It is well clarified in our previous paper[6] that the dark spots in the micrograph taken without the polarizer and analyzer or with only one of the polarizer or analyzer correspond to the disclination lines oriented normal to the plane of the thin films. Since the dynamics of the disclination lines are relatively slow, one can clearly see that the dark spots correspond to the disclination lines by superimposing micrographs a and b on top of each other. Furthermore the strength, S, of the disclination lines in the micrograph field is found to be $^1/_2$ by observing the rotation of the dark brushes when the analyzer and polarizer are rotated together, maintaining a crossed position. Disclinations with strength of $S = \pm 1$ were occasionally found in other fields, but the disclinations with $S = \pm^1/_2$ were the most abundant, which is reasonable because the elastic energy of the disclination is proportional to S^2.

Figure 2 shows a typical time evolution of Schlieren texture (a) and corresponding H_v (b) and V_v (c) light-scattering patterns at 2, 10, and 30 s after the T jump of the as-cast films of X-7G

0024-9297/89/2222-0422$01.50/0

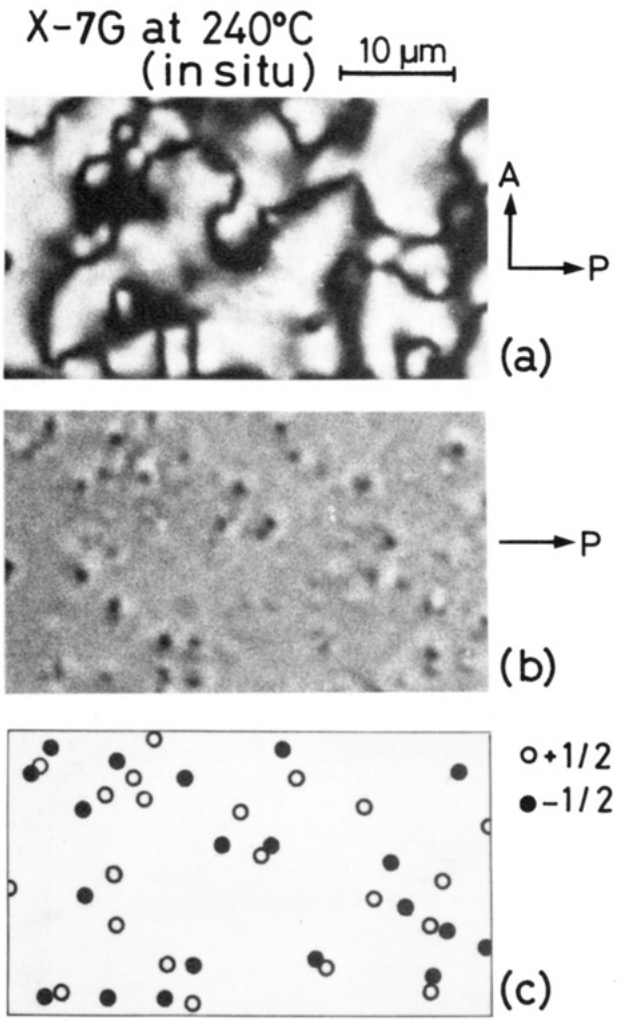

Figure 1. Analyses of Schlieren texture developed by isothermal annealing of the as-cast films of X-7G at 240 °C for 82 s (b and c) and 90 s (a): (a) crossed Nicols; (b) horizontal polarizer alone; (c) spatial distribution of the disclinations and their strength.

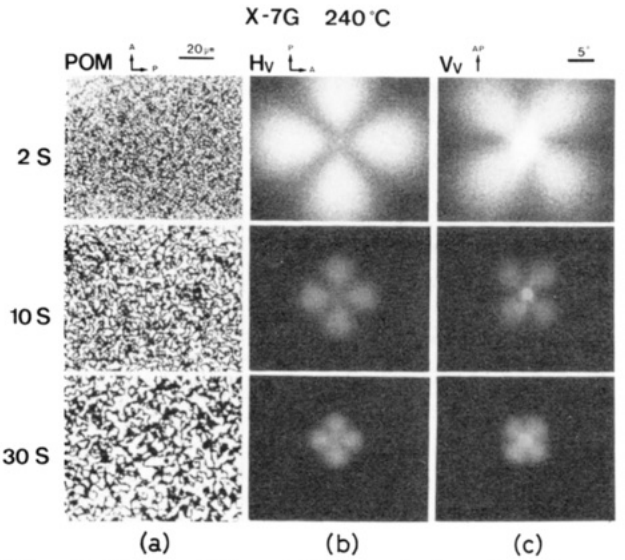

Figure 2. Time evolution of Schlieren texture (a) and corresponding changes of H_v (b) and V_v (c) scattering patterns during isothermal annealing of X-7G as-cast films at 240 °C. P and A designate polarization direction of the polarizer and analyzer.

to 240 °C. After the T jump the initially homogeneous and optically isotropic films are quite rapidly transformed into the nematic liquid crystal phase with a large number of disclinations. The figure indicates the ordering process during the isothermal annealing in which the free energy of the system is relaxed as a consequence of the annihilation of the disclinations with time and hence of coarsening of the Schlieren texture with time. The coarsening involves an increase in the average distance d between neighboring disclinations as given by[6]

$$d \sim t^{0.35} \tag{1}$$

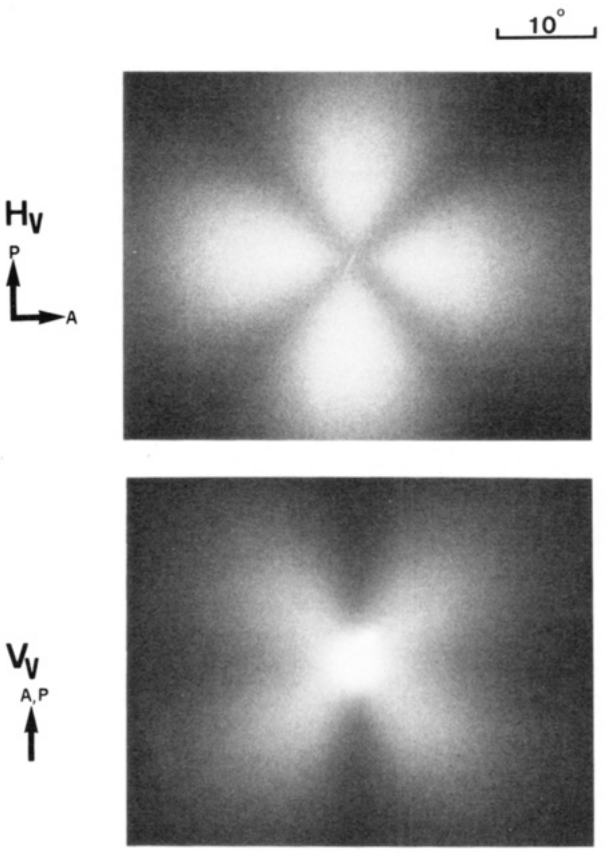

Figure 3. H_v (a, top) and V_v (b, bottom) scattering patterns from nematic liquid crystals of the semiflexible aromatic polyester.

The Schlieren texture was found to give unique H_v and V_v small-angle light-scattering patterns. These have a maximum intensity at scattering angle $\theta = \theta_{max}$. They have an azimuthal angle (μ) dependence with a 4-fold symmetry with maximum intensities at $\mu = \mu_{max}$, μ_{max} being an integer multiples of $\mu = 90°$ for H_v and odd multiples of $\mu = 45°$ for V_v. The azimuthal angle dependence of H_v and V_v with μ is invariant with time, but θ_{max} decreases with time during the ordering process. The latter is nicely correlated with the coarsening of the Schlieren texture and suggests an increase of the correlation length d in the orientation fluctuations of the director field caused by many-body interactions of the disclinations. The origin of this unique scattering will be discussed in sections III and IV.

Figure 3 shows (a) H_v and (b) V_v small-angle light-scattering patterns from the semiflexible aromatic polyester quenched from the nematic phase. The patterns have the same characteristics as those shown in Figure 2 from the copolyester X-7G. Thus the unique patterns may reflect the universal nature of the thermotropic nematic polymer liquid crystals.

Figure 4 shows schematically the disclinations of $S = \pm^1/_2$ and ± 1 found generally for the nematics where the disclination lines located at an origin of the $0xyz$ coordinate are normal to the plane of the paper in all cases and the directors change their orientation along the lines or at a fixed angle ϕ_0 with respect to the lines drawn around the disclinations. The spatial distribution of these disclinations should result in the observed Schlieren texture and would generally be responsible for the small-angle light scattering. Under crossed Nicols, a number of dark brushes which is equal to $4|S|$ emanates from each disclination line, the dark brushes corresponding to the region where the optical axis is parallel to one of the Nicols. Thus the micrograph shown in Figure 1a indicates that the field under examination is exclusively composed of disclination with $S = \pm^1/_2$.

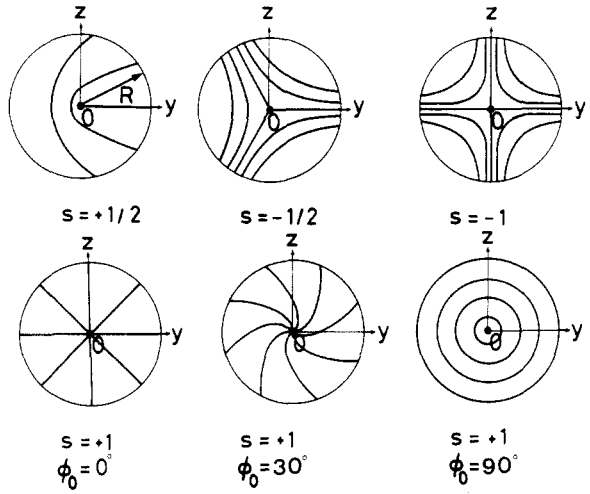

Figure 4. Various types of disclinations in nematic liquid crystals, models of isolated disks of radius R with a single disclination at the center, and definition of $0xyz$ coordinates fixed to the disk.

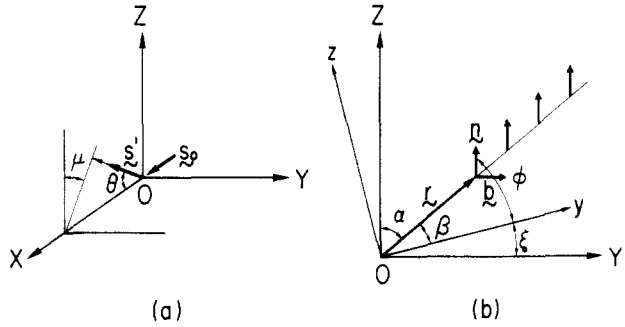

Figure 5. Coordinate systems fixed to the laboratory $0XYZ$ and the liquid crystal disk $0xyz$ and definitions of various vectors and angles. $0Z$: vertical axis. $\mathbf{s}_0$ and $\mathbf{s}'$ are unit vectors along incident and scattered beams, $\mathbf{n}$ is the director (unit vector along the optical axis), and $\mathbf{r}$ is the position vector of a scattering element in the disk. θ and μ are the scattering and azimuthal angles, respectively. ξ is an angle specifying orientation of the disk with the laboratory-fixed coordinate.

In the next section, we will discuss the small-angle scattering from a single isolated disk of radius R with orientation fluctuations of the director around its disclination located at its center as the simplest possible model (see Figure 4). The disks may have various disclinations as shown in Figure 4 and the scattering will be investigated for normal incidence to the disk.

III. Scattering Theory

III-1. Model of Isolated Disk with a Single Disclination at the Center. Figure 5 shows the coordinate systems for the scattering experiments (a) and the calculation of the scattering from the model (b). $0XYZ$ is the Cartesian coordinate fixed to the laboratory; $0X$ being the propagation direction of the incident beam (specified by the unit vector $\mathbf{s}_0$) and $0Z$ being the vertical direction. The scattering pattern or profile is recorded by the two-dimensional detector placed normal to $0X$ as a function of the scattering angle θ and azimuthal angle μ as shown in Figure 5a.

The isolated disk has a radius R and a single disclination of strength S and ϕ_0 (the angle between the optical axis and the line drawn around the disclination) at the center of the disk. We choose the Cartesian coordinate $0xyz$ fixed to the disk as shown in Figure 5b where the $0x$ axis is normal to the disk and parallel to the disclination line. The plane of the disk $0yz$ lies in the plane of $0YZ$. One of the axes of the disk, e.g., the $0y$ axis, makes an angle ξ with respect to the $0Y$ axis fixed to the laboratory. The angle ξ may be uniformly distributed (for a random orientation) or distributed around a particular value of ξ_0 (for a preferential orientation). The angle ξ and its distribution are insignificant for the disclinations of $S = +1$ because the director field is circularly symmetric. In other words, an averaging for orientation is not necessary for the scattering intensity calculation. Moreoever for the disclinations of $S = \pm^1/_2$ and $S = -1$, the geometry of the problem as well as the mathematical derivations can be simplified without loosing generality by letting the $0y$ axis coincide with the $0Y$ axis fixed to the laboratory (Figure 5b). In other words, instead of averaging with ξ, one can average with ϕ_0 to calculate the scattering intensity.

The director field $\mathbf{n}(\mathbf{r})$ within the disk is given by

$$\phi(\mathbf{r}) = \phi(r,\beta) = S\beta + \phi_0 \tag{2}$$

where as shown in Figure 5, ϕ is the angle specifying orientation of the director $\mathbf{n}(\mathbf{r})$ at $\mathbf{r}$ with respect to the $0y$ axis, S is the strength of the disclination, β specifies the orientation of the vector $\mathbf{r}$ with respect to the $0y$ axis, and ϕ_0 is the constant value. The director field $\mathbf{n}(\mathbf{r})$ is assumed to lie in the plane $0yz$, parallel to the film surfaces.

III-2. Physical Intuitions about Small-Angle Scattering from Nematics. Before going into detailed calculations of the scattering functions for the isolated disk with a single disclination at its center, it would be quite useful to gain some intuition about the physics of the scattering phenomenon from the disk.

In the context of Rayleigh–Gans–Born scattering, the scattering amplitudes under H_v and V_v polarization conditions are given by

$$E_{Ab} = \sum_j E_{j,Ab} \tag{3}$$

$$E_{j,Ab} = C_1(\mathbf{M}\cdot\mathbf{O})_{Ab} \exp\{i\mathbf{q}\cdot\mathbf{r}_j\} \tag{4}$$

where A_b designates either H_v or V_v polarization conditions of the scattering experiments; E_{Ab} is the scattering amplitude under A_b polarization; $(\mathbf{M}\cdot\mathbf{O})_{Ab}$ is the corresponding induced dipole moment; $\mathbf{q}$ is the scattering vector whose magnitude is given by

$$|\mathbf{q}| = (4\pi/\lambda) \sin(\theta/2) \tag{5}$$

where λ and θ are the wavelength of the incident beam and the scattering angle in the medium, respectively; $E_{j,Ab}$ is the scattering amplitude from the jth scattering element located at $\mathbf{r}_j$ from the center; and C_1 is a proportional constant independent of $\mathbf{q}$.

Let us first consider the total scattering amplitudes under H_v and V_v (designated respectively $E_{4,Hv}$ and $E_{4,Vv}$) from the four scattering elements R_1–R_4 located at $\mathbf{r}_1$–$\mathbf{r}_4$ from the center for the disclinations of $S = +^1/_2$ and $\phi_0 = 0°$ (a) and $S = +1$ and $\phi_0 = 0°$ (b) as shown in Figure 6. For simplicity, we assume here the disk has a particular orientation with its axis $0y$ along the laboratory fixed coordinate $0Y$ (see Figure 5).

a. Case of $S = ^1/_2$ and $\phi_0 = 0°$. The induced dipole moments under H_v and V_v polarizations for the disk with $S = +^1/_2$ and $\phi_0 = 0°$ are given by

$$(\mathbf{M}\cdot\mathbf{O})_{Hv,S=1/2} = C_2(\alpha_1 - \alpha_2) \sin(\beta/2) \cos(\beta/2) = (1/2)C_2(\alpha_1 - \alpha_2) \sin\beta \tag{6}$$

and

$$(\mathbf{M}\cdot\mathbf{O})_{Vv,S=1/2} = C_3[\alpha_1^2 \sin^2(\beta/2) + \alpha_2^2 \cos^2(\beta/2)] = (1/2)C_3[-(\alpha_1 - \alpha_2) \cos\beta + (\alpha_1 + \alpha_2)] \tag{7}$$

where C_2 and C_3 are constants related to the absolute intensity and α_1 and α_2 are the polarizabilities parallel and perpendicular to the director, respectively. Equations 6 and 7 are obtained similarly to the calculation of the in-

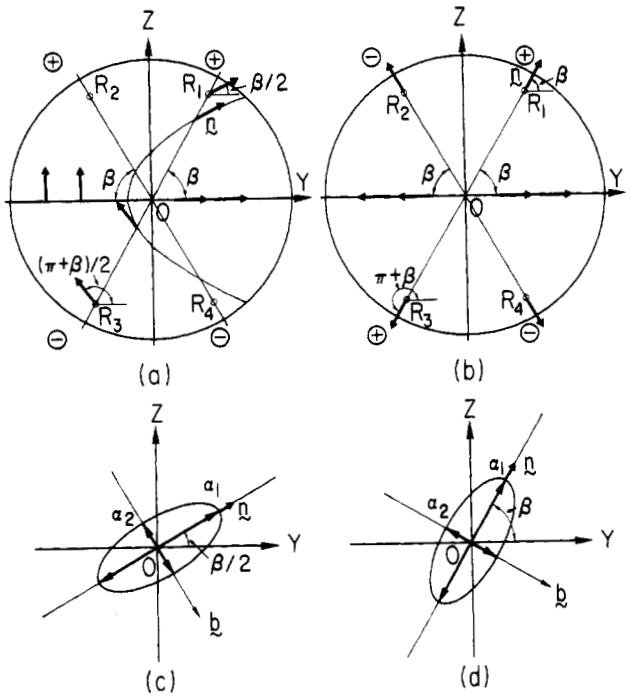

Figure 6. Diagrams showing the nature of scattering from the disk with the disclination of $S = +^1/_2$ and $\Phi_0 = 0°$ (a and c) and $S = +1$ and $\Phi_0 = 0°$ (b and d). (a) and (b) show spatial variation in orientation of the director in the disk, particularly at four positions $\mathbf{r}_1$–$\mathbf{r}_4$ possessing a certain symmetry. (c) and (d) show orientation of the directors at $\mathbf{r}_1$.

duced dipole moment for a two-dimensional spherulite[7] by noting that all the directors at the positions specified by the angle β in the disk make an orientational angle $\beta/2$ with respect to the horizontal axis $0Y$.

From eq 3–7, it follows that

$$E_{4,\mathrm{Hv}} = (1/2)C_2(\alpha_1 - \alpha_2)\{\sin\beta\exp(i\mathbf{q}\cdot\mathbf{r}_1) + \sin\beta\exp(i\mathbf{q}\cdot\mathbf{r}_2) - \sin\beta\exp(i\mathbf{q}\cdot\mathbf{r}_3) - \sin\beta\exp(i\mathbf{q}\cdot\mathbf{r}_4)\} \quad (8)$$

It is important to note in eq 8 that the disk itself is centrosymmetric for its density fluctuations but its scattering power within the disk is *not centrosymmetic* under $\mathrm{H_v}$ polarization, i.e.,

$$(\mathbf{M}\cdot\mathbf{O})_{\mathrm{Hv},\mathbf{r}_1} \neq (\mathbf{M}\cdot\mathbf{O})_{\mathrm{Hv},\mathbf{r}_3},\ (\mathbf{M}\cdot\mathbf{O})_{\mathrm{Hv},\mathbf{r}_2} \neq (\mathbf{M}\cdot\mathbf{O})_{\mathrm{Hv},\mathbf{r}_4} \quad (9)$$

so that one should note in eq 3 and 4

$$\sum_j (\mathbf{M}_j\cdot\mathbf{O})_{Ab}\exp\{i\mathbf{q}\cdot\mathbf{r}_j\} \neq \sum_j (\mathbf{M}_j\cdot\mathbf{O})_{Ab}\cos(\mathbf{q}\cdot\mathbf{r}_j) \quad (10)$$

i.e., the term $\{i\sin(\mathbf{q}\cdot\mathbf{r}_j)\}$ in $\exp\{i\mathbf{q}\cdot\mathbf{r}_j\}$ has to be maintained. For all the $\mathbf{q}$ vectors along the Y axis, i.e., for the scattering at $\mu = 90°$ and 270°

$$\mathbf{q}\cdot\mathbf{r}_1 = \mathbf{q}\cdot\mathbf{r}_4, \qquad \mathbf{q}\cdot\mathbf{r}_2 = \mathbf{q}\cdot\mathbf{r}_3 \quad (11)$$

and hence $E_{4,\mathrm{Hv}} = 0$. This implies no $\mathrm{H_v}$ scattering at $\mu = 90°$ and 270° from the disk as a whole, since the disk is composed of an assembly of such four scattering elements as R_1–R_4. Similarly for all $\mathbf{q}$ vectors along the Z axis, i.e., at $\mu = 0°$ or 180°

$$E_{4,\mathrm{Hv}} = 2C_2(\alpha_1 - \alpha_2)i\sin\beta\sin(\mathbf{q}\cdot\mathbf{r}_1) \quad (12)$$

Thus the $\mathrm{H_v}$ scattered intensity becomes maximum at $\mu = 0°$ and 180° with respect to μ. The $\mathrm{H_v}$ scattering pattern would have 2-fold symmetry with a maximum intensity at a particular θ ($=\theta_{1/2}$) and at $\mu = 0°$ and 180° as schematically shown in Figure 7a.

$\mathrm{V_v}$ scattering depends on two terms, i.e., the term which depends on orientation ($\cos\beta$) and the term which depends only on polarizability ($\alpha_1 + \alpha_2$) (the density term). The

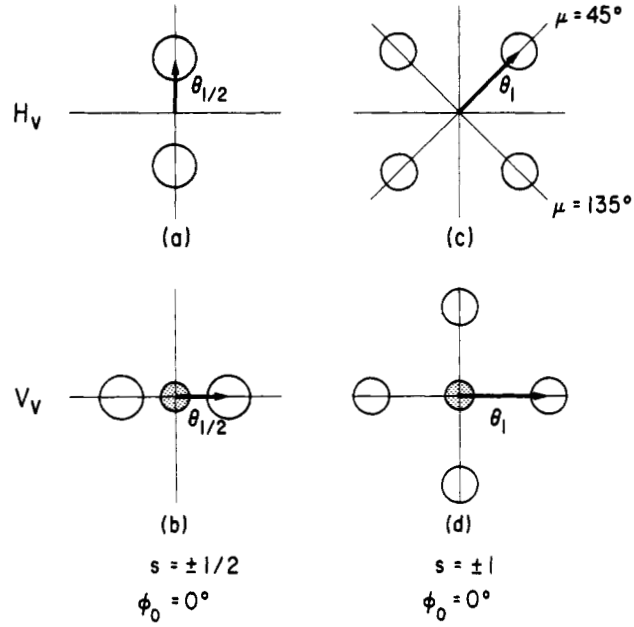

Figure 7. Schematic illustrations of $\mathrm{H_v}$ and $\mathrm{V_v}$ scattering patterns for the disk with $S = \pm^1/_2$ and $\Phi_0 = 0°$ (a and b) and with $S = \pm1$ and $\Phi_0 = 0°$ (c and d). The hatched and unhatched lobes in the $\mathrm{V_v}$ pattern designate, respectively, the density and orientation contributions to the scattering. $\theta_{1/2}$ and θ_1 satisfy eq 29 and 36, respectively.

density term gives the diffuse scattering with a circularly symmetric intensity distribution with μ and with a maximum intensity at $\theta = 0$ (as drawn schematically by the lobe shaded in Figure 7b,d). The orientation-dependent term gives

$$E_{4,\mathrm{Vv,orient}} = (1/2)C_3(\alpha_1 - \alpha_2)\{-\cos\beta\exp(i\mathbf{q}\cdot\mathbf{r}_1) + \cos\beta\exp(i\mathbf{q}\cdot\mathbf{r}_2) + \cos\beta\exp(i\mathbf{q}\cdot\mathbf{r}_3) - \cos\beta\exp(i\mathbf{q}\cdot\mathbf{r}_4)\} \quad (13)$$

Again the orientation-dependent term is not centrosymmetric so that one should note the inequality of eq 10.

$$E_{4,\mathrm{Vv,orient}} = 0$$

for all $\mathbf{q}$ vectors along the Z axis ($\mu = 0°$, 180°) (14a)

$$E_{4,\mathrm{Vv,orient}} = -2C_3 i(\alpha_1 - \alpha_2)\cos\beta\sin(\mathbf{q}\cdot\mathbf{r}_1)$$

for all $\mathbf{q}$ vectors along the Y axis ($\mu = 90°$, 270°) (14b)

Thus the orientation-dependent term gives the $\mathrm{V_v}$ pattern with a 2-fold symmetry having a maximum intensity at $\mu = 90°$ and 270° with μ and at $\theta = \theta_{1/2}$, as shown schematically in Figure 7b by the unshaded lobes.

b. Case of $S = 1$ and $\phi_0 = 0°$. The induced dipole moments are given by

$$(\mathbf{M}\cdot\mathbf{O})_{\mathrm{Hv},S=+1} = (1/2)C_2(\alpha_1 - \alpha_2)\sin 2\beta \quad (15)$$

$$(\mathbf{M}\cdot\mathbf{O})_{\mathrm{Vv},S=+1} = (1/2)C_3[-(\alpha_1 - \alpha_2)\cos 2\beta + (\alpha_1 + \alpha_2)] \quad (16)$$

This case is identical with the scattering from a two-dimensional spherulite with the optical axis oriented along the radial direction of the spherulite.[7] In this case the disk has a centrosymmetric scattering power under both $\mathrm{H_v}$ and $\mathrm{V_v}$ polarizations, and hence inequality of eq 10 can be replaced by equality.

$$E_{4,\mathrm{Hv}} = (1/2)C_2(\alpha_1 - \alpha_2)\{\sin 2\beta\cos(\mathbf{q}\cdot\mathbf{r}_1) - \sin 2\beta\cos(\mathbf{q}\cdot\mathbf{r}_2) + \sin 2\beta\cos(\mathbf{q}\cdot\mathbf{r}_3) - \sin 2\beta\cos(\mathbf{q}\cdot\mathbf{r}_4)\} \quad (17)$$

Obviously

$$E_{4,\mathrm{Hv}} = 0 \qquad \text{(for all } \mathbf{q} \text{ vectors along } 0Y \text{ and } 0Z \text{ axes)} \quad (18)$$

Thus the H_v scattering gives a pattern, schematically shown in Figure 7c, having a 4-fold symmetry with respect to μ and with maximum intensity at odd multiples of μ = 45° and zero intensities at integer multiples of μ = 90°. The orientation-dependent V_v scattering is given by

$$E_{4,Vv} = -(1/2)C_3(\alpha_1 - \alpha_2)\cos 2\beta \sum_{i=1}^{4} \exp(i\mathbf{q}\cdot\mathbf{r}_j) \quad (19)$$

Thus the orientation-dependent term of V_v scattering does not vanish to zero at all $\mathbf{q}$ vectors. The corresponding V_v intensity should have a 4-fold symmetry with μ, having maximum intensity at μ = 0°, 90°, 180°, and 270°, the μ-dependence of which is schematically drawn in Figure 7d (the unshaded lobes).

III-3. Scattering Functions from an Isolated Disk with a Single Disclination at Its Center. Rigourous calculations of the scattering functions from the systems as defined in sections III-1 and -2 give the scattering amplitudes E_{Hv} and E_{Vv} for H_v and V_v scattering

$$E_{Hv} = -\pi K(\alpha_1 - \alpha_2)E_0 \cos \rho_2 \sin [S(\pi - 2\mu) + 2\phi_0] \times (R/W)^2\{(\delta|S| - 1)\{2[1 - J_0(W)] - WJ_1(W)\} + i\delta(|S| - 1/2)I_1(W)\} \quad (20)$$

where

$$W = (2\pi/\lambda)R \sin \theta \quad (21)$$

$\delta(x)$ is a step function defined as

$$\delta(x) = 1 \quad \text{if } x = 0$$
$$= 0 \quad \text{otherwise} \quad (22)$$

and $I_1(W)$ is given by

$$I_1(W) \equiv \int_0^W J_1(x)x\, dx \quad (23)$$

J_0 and J_1 are the Bessel functions of the first kind, E_0 is the amplitude of the incident beam, K is a constant related to the absolute scattered intensity, and $\cos \rho_2$ is given by[7]

$$\cos \rho_2 = \cos \theta[\cos^2 \theta + \sin^2 \theta \sin^2 \mu]^{-1/2} \quad (24)$$

which is equal to unity at small θ.

$$E_{Vv} = -\pi K E_0 \cos \rho_1 (R/W)^2\{(\alpha_1 - \alpha_2)\cos [S(\pi - 2\mu) + 2\phi_0]\delta(|S| - 1)[2[1 - J_0(W)] - WJ_1(W)] + i(\alpha_1 - \alpha_2)\cos [S(\pi - 2\mu) + 2\phi_0]\delta(|S| - \tfrac{1}{2})I_1(W) - (\alpha_1 + \alpha_2 - 2\alpha_s)WJ_1(W)\} \quad (25)$$

where α_s is the polarizability of the medium surrounding the disk, and

$$\cos \rho_1 = \cos \theta[\cos^2 \theta + \sin^2 \theta \cos^2 \mu]^{-1/2} \quad (26)$$

a. Case of $S = {}^1/_2$. Substituting $S = {}^1/_2$ into eq 20 and 25 and taking $E_{Hv}E_{Hv}^*$ and $E_{Vv}E_{Vv}^*$ (* being the conjugated complex), one obtains the corresponding scattering intensity for H_v and V_v

$$I_{Hv}(S=\tfrac{1}{2}) = \pi^2K^2E_0^2(\alpha_1 - \alpha_2)^2 \cos^2 \rho_2 \cos^2 (\mu - 2\phi_0)(R/W)^4I_1(W)^2 \quad (27)$$

$$I_{Vv}(S=\tfrac{1}{2}) = \pi^2K^2E_0^2 \cos^2 \rho_1 (R/W)^4\{(\alpha_1 - \alpha_2)^2 \times \sin^2 (\mu - 2\phi_0)I_1(W)^2 + (\alpha_1 + \alpha_2 - 2\alpha_s)^2W^2J_1(W)^2\} \quad (28)$$

where the "effective" polarizabilities of the surroundings for α_1 and α_2 are assumed to be equal to α_s.

In the case when ϕ_0 = 0°, the dependences of H_v and V_v scattering patterns on the azimuthal angle μ are given respectively by $\cos^2 \mu$ and $\sin^2 \mu$, having a 2-fold symmetry with maximum intensities at μ = 0° and 180° and at μ = 90° and 270°, respectively, as schematically illustrated in Figure 7a,b. The angular dependence of H_v and V_v scattering with the scattering angle θ can be determined by $P_1(W) \equiv I_1(W)^2/W^4$ and $P_3(W) \equiv J_1(W)^2/W^2$, which are given in Figure 8. Thus the H_v scattering has a maximum intensity at $\theta_{1/2}$ satisfying

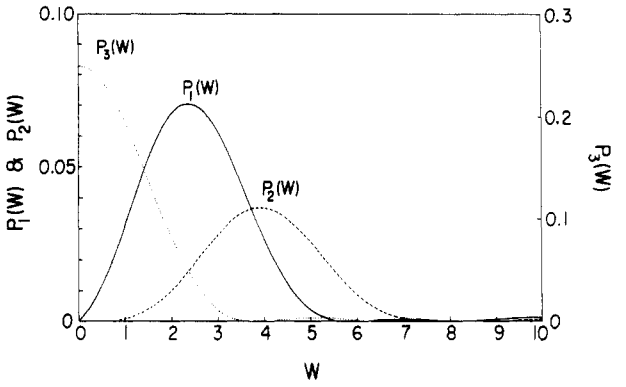

Figure 8. Functions $P_1(W)$, $P_2(W)$, and $P_3(W)$ which determine the angular dependence of H_v and V_v scattering intensity with θ. $P_1(W) \equiv I_1(W)^2/W^4$, $P_2(W) \equiv \{2[1 - J_0(W)] - WJ_1(W)\}^2/W^4$, and $P_3(W) \equiv J_1(W)^2/W^2$.

$$W_{max} = (2\pi/\lambda)R \sin \theta_{1/2} = 2.35 \quad (29)$$

The V_v scattering arising from the orientation or anisotropy term $(\alpha_1 - \alpha_2)$ has a maximum at $\theta_{1/2}$, but that from the density term $(\alpha_1 + \alpha_2 - 2\alpha_2)$ has a maximum at θ = 0 as shown in Figure 7b and Figure 8.

If the disk has a nonzero value of ϕ_0, the azimuthal angle dependence of H_v and V_v scattering patterns is given by $\cos^2 (\mu - 2\phi_0)$ and $\sin^2 (\mu - 2\phi_0)$, respectively, and hence the patterns are obtained by a rotation of the patterns for ϕ_0 = 0° through the angle $2\phi_0$ in a clockwise direction around the incident beam axis. If the orientation of the disk is random, $\cos^2 (\mu - 2\phi_0)$ and $\sin^2 (\mu - 2\phi_0)$ should be replaced by

$$\langle \cos^2 (\mu - 2\phi_0)\rangle_{av} = \langle \sin^2 (\mu - 2\phi_0)\rangle_{av} = 1/2 \quad (30)$$

where $\langle\ \rangle_{av}$ designates an average over all possible ϕ_0. Hence the H_v and V_v patterns become independent of μ as shown in Figure 9a.

b. Case of $S = {}^{-1}/_2$. Similarly to the case of $S = {}^1/_2$, the H_v and V_v scattering intensities are given by

$$I_{Hv}(S=-\tfrac{1}{2}) = \pi^2K^2(\alpha_1 - \alpha_2)^2E_0^2 \cos^2 \rho_2 \cos^2 (\mu + 2\phi_0)(R/W)^4I_1(W)^2 \quad (31)$$

and

$$I_{Vv}(S=-\tfrac{1}{2}) = \pi^2K^2E_0^2 \cos^2 \rho_1 (R/W)^4\{(\alpha_1 - \alpha_2)^2 \times \sin^2 (\mu + 2\phi_0)I_1(W)^2 + (\alpha_1 + \alpha_2 - 2\alpha_s)^2W^2J_1(W)^2\} \quad (32)$$

Thus in the case of ϕ_0 = 0°, the patterns have the same angular dependence with θ and μ as those for $S = {}^1/_2$, as shown in Figure 7a,b. If $\phi_0 \neq 0°$, the H_v and V_v patterns should have μ dependence, which are rotated through the angle $2\phi_0$ in the counterclockwise direction with respect to the patterns for ϕ_0 = 0°. If the disk has a random orientation, the H_v and V_v patterns are angularly independent with μ and are identical with those for $S = {}^1/_2$, as given in Figure 9a, because

$$\langle \cos^2 (\mu + 2\phi_0)\rangle_{av} = \langle \sin^2 (\mu + 2\phi_0)\rangle_{av} = 1/2 \quad (33)$$

c. Case of S = 1.

$$I_{Hv}(S=1) = \pi^2K^2(\alpha_1 - \alpha_2)^2E_0^2 \cos^2 \rho_2 \sin^2 2(\mu - \phi_0) \times (R/W)^4\{2[1 - J_0(W)] - WJ_1(W)\}^2 \quad (34)$$

$$I_{Vv}(S=1) = \pi^2K^2E_0^2 \cos^2 \rho_1 (R/W)^4\{(\alpha_1 - \alpha_2) \times \cos 2(\mu - \phi_0)[2[1 - J_0(W)] - WJ_1(W)] - (\alpha_1 + \alpha_2 - 2\alpha_s)WJ_1(W)\}^2 \quad (35)$$

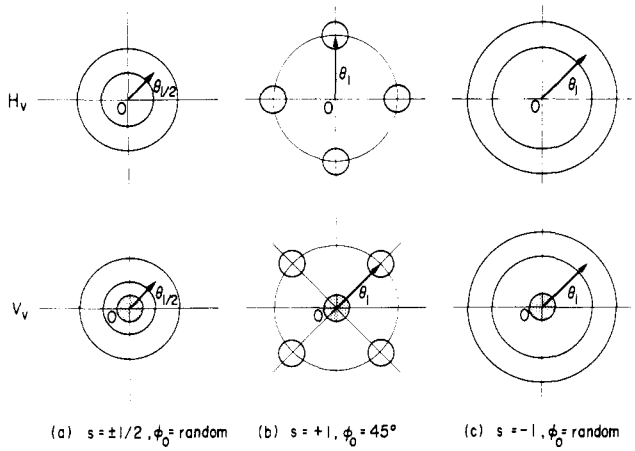

Figure 9. Schematic illustrations of H_v and V_v scattering patterns for the disk with $S = \pm^1/_2$ and a random orientation with ϕ_0 (a), the disk with $S = +1$ and $\phi_0 = 45°$ (b), and the disk with $S = -1$ and a random orientation with ϕ_0 (c).

The equations are identical with those for the two-dimensional spherulites with the optical axis in the plane of the spherulite and inclined by the angle ϕ_0 with respect to the spherulite radius.[7] In this case the director field $\mathbf{n}(\mathbf{r})$ is circularly symmetric so that the scattering does not depend on ξ (Figure 5b).

In the case when $\phi_0 = 0°$, the Hv scattering pattern has a 4-fold symmetry, with μ having a maximum intensity at odd multiples of $\mu = 45°$, as shown in Figure 7c. It has a maximum intensity at $\theta = \theta_1$, satisfying

$$W_{max} = (2\pi/\lambda)R \sin \theta_1 = 3.9 \quad (36)$$

as shown in Figures 7 and 8 and as previously indicated.[7] The orientation-dependent term of the V_v scattering has a 2-fold symmetry with μ, as it depends on $\cos 2\mu$, while the density-dependent term of the V_v scattering is independent of μ. If the density contribution is small compared with the orientation contribution, $I_{Vv} \sim \cos^2 2\mu$ and hence it has a 4-fold symmetry with μ, having a maximum intensity at integer multiples of $\mu = 90°$, as shown in Figure 7d with the unshaded lobes.

The patterns for the case of $\phi_0 \neq 0°$ are obtained by the rotation of the patterns for the case of $\phi_0 = 0°$ by the angle ϕ_0 in a clockwise direction around the incident beam axis, the case of $\phi_0 = 45°$ being schematically shown in Figure 9b.

d. Case of $S = -1$.

$$I_{Hv}(S=-1) = \pi^2K^2(\alpha_1 - \alpha_2)^2E_0^2 \cos^2 \rho_2 \times \sin^2 2(\mu + \phi_0)(R/W)^4\{2[1 - J_0(W)] - WJ_1(W)\}^2 \quad (37)$$

$$I_{Vv}(S=-1) = \pi^2K^2E_0^2 \cos^2 \rho_1(R/W)^4\{(\alpha_1 - \alpha_2) \times \cos 2(\mu + \phi_0)[2[1 - J_0(W)] - WJ_1(W)] - (\alpha_1 + \alpha_2 - 2\alpha_s)WJ_1(W)\}^2 \quad (38)$$

Thus in the case of $\phi_0 = 0°$, the H_v and V_v scattering patterns are identical with those for $S = 1$ and $\phi_0 = 0°$, as shown in parts c and d of Figure 7. In the case of $\phi_0 \neq 0°$, the H_v and V_v patterns are obtained by rotating the corresponding patterns for $\phi_0 = 0°$ through the angle ϕ_0 in the counterclockwise direction around the incident beam axis. If the disk has a random orientation, then

$$\langle \sin^2 2(\mu + \phi_0) \rangle_{av} = \langle \cos^2 2(\mu + \phi_0) \rangle_{av} = 1/2 \quad (39)$$

so that the H_v and V_v scattering patterns become independent of μ as shown in Figure 9c. The V_v scattering for the random orientation is given by

$$I_{Vv}(S=-1)_{rand} = \pi^2K^2E_0^2 \cos^2 \rho_1(R/W)^4\{1/2(\alpha_1 - \alpha_2)^2[2[1 - J_0(W)] - WJ_1(W)]^2 + (\alpha_1 + \alpha_2 - 2\alpha_s)^2W^2J_1(W)^2\} \quad (40)$$

III-4. Comparison with the Experimental Patterns. The experimental H_v and V_v scattering patterns, having a maximum scattering intensity at $\theta = \theta_{max}$ and at integer multiples of $\mu = 90°$ (for H_v) and at odd multiples of $\mu = 45°$ (for V_v) as shown in Figure 2, might be described in terms of an isolated disk with a disclination of $S = +1$ and $\phi_0 = 45°$ at the center, as shown in Figure 9b.

The disks with disclinations of other kinds cannot account for the experimental patterns. However, the interpretation of the scattering patterns with the isolated disk of $S = +1$ and $\phi_0 = 45°$ is not reasonable, since the analysis of the Schlieren texture indicates that most of the disclinations found in the X-7G films are those of $S = \pm^1/_2$. The disks with the disclinations of $S = \pm^1/_2$ predict scattering patterns as shown in Figures 7a,b and 9a and hence cannot account for the experimental patterns.

The discrepancy between the predicted and experimental scattering patterns deserves further consideration. In the next section we will suggest a possible and qualitative interpretation on the discrepancy on the basis of many-body interactions of disclinations.

IV. Many-Body Interactions of Disclinations

The description of the scattering patterns based upon a single and isolated disk with a single disclination at its center is certainly an oversimplification, as was discussed in the previous section, III-4. The patterns should be described on the basis of many-body interactions of the disclinations and the resulting fluctuation of the director field $\mathbf{n}(\mathbf{r})$.

For example, Figure 10a describes two-body interactions of the disclinations with $S = \pm^1/_2$ separated at a distance of $2R + L$. Here we assume that the system can be treated as a random assembly of the domain composed of a set of the two disclinations (i.e., the two disks and the intermediary region M). If the intermediary region (shaded region with length L) has much larger area than the area occupied by the two disks, the scattering from such a domain primarily arises from the intermediary region M. Furthermore the scattering from such region is well described in terms of the scattering from an optically anisotropic rod[8-10] and is well-known as "rodlike scattering" or "anisotropic rodlike scattering."

The anisotropic rodlike scattering predicts a monotonic intensity decrease with increasing scattering angle θ as schematically shown in Figure 10b,c, no maximum being predicted.[8-12] It gives rise to the μ dependence as schematically shown in Figure 10b,c, depending upon the orientation angle ϕ_0 which the director makes with respect to the rod axis (see Figure 10a) and upon asymmetry of the shape, i.e., an aspect ratio of $L/2R$.[10,11] The rod model with $\phi_0 = \pm 45°$ originating from the two-body interactions can account for the μ dependence of the experimental patterns.

Figure 11 describes three-body interactions of disclinations with $S = \pm^1/_2$. The system is now assumed to be treated as a random assembly of domains composed of sets of the three disclinations (i.e., the three disks and the two intermediary regions M_1 and M_2). Again if $L \gg R$, the scattering dominantly arises from the intermediary regions M_1 and M_2. The "inter-rod" interference[12] between the rodlike scattering from the region M_1 and M_2 separated by a distance d may cause the scattering maximum at the

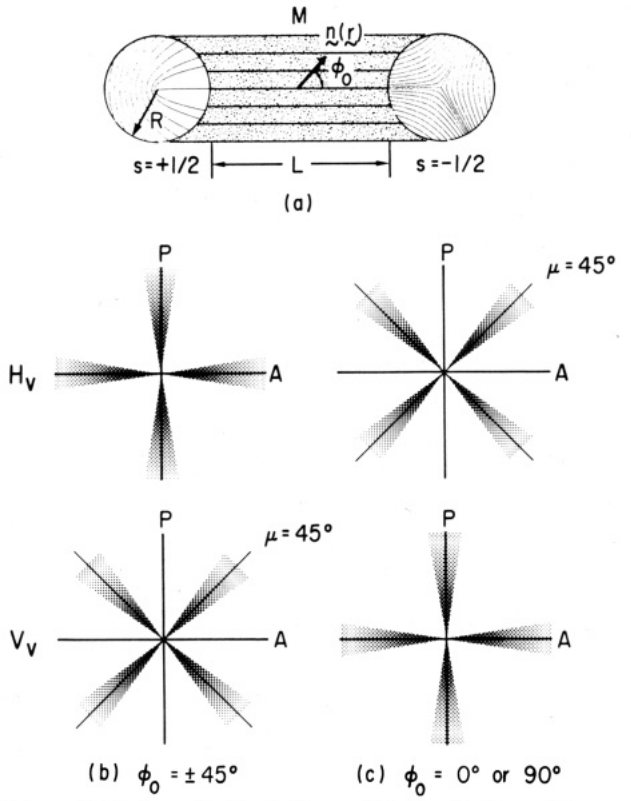

Figure 10. Schematic illustrations of the two-body model composed of the two disks with $S = \pm^1/_2$ and the intermediary regions M (a) and corresponding H_v and V_v patterns for $\phi_0 = \pm 45°$ (b) and $\phi_0 = 0°$ or 90° (c). The volume of the intermediary region M which gives rise to the anisotropic rodlike scattering is assumed to be much larger than the volume of the two disks with $S = \pm^1/_2$ disclinations, and hence the intermediary volume gives a dominant contribution to the net scattering. It should be noted that the scattered intensity decreases monotonically with increasing θ.

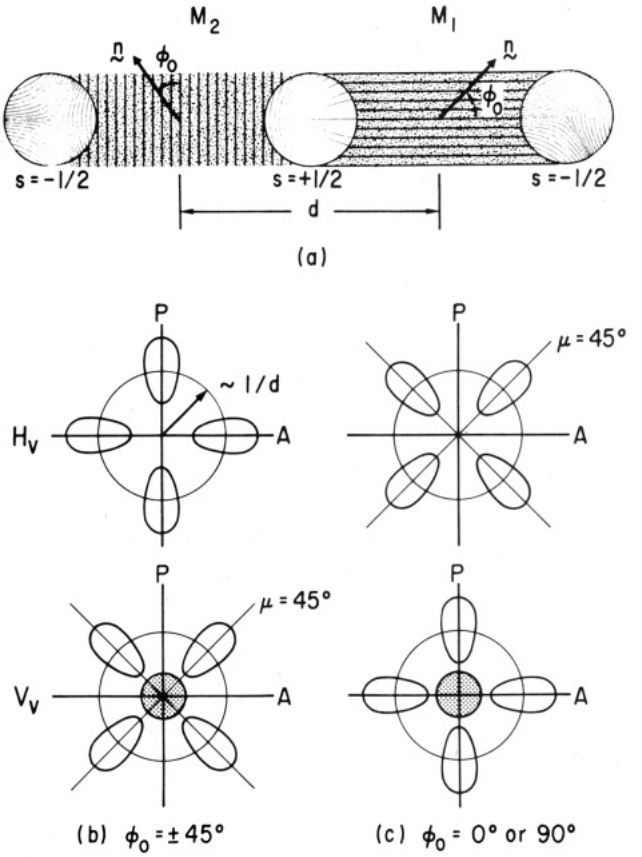

Figure 11. Schematic illustrations of the three-body model composed of three disks with $S = \pm^1/_2$ and the intermediary regions M_1 and M_2 (a) and corresponding H_v and V_v scattering patterns for $\phi_0 = 45°$ (b) and $\phi_0 = 0°$ or 90° (c). Interference between the rodlike scattering from the two intermediary regions M_1 and M_2 may give rise to the scattering maximum at the scattering angle proportional to $1/d$ (distance between M_1 and M_2).

scattering angle reciprocally proportional to $1/d$ as schematically shown in Figure 11b,c. Thus the three-body model may qualitatively account for the experimental scattering patterns.

The two-body or three-body model can account for the experimental scattering patterns better than the isolated disk model. However, the two- and three-body models have difficulties in that the interstitial region between the domains was not properly treated by a random assembly of the models. Figure 12 shows schematically an example of a multibody model to make the difficulties of the interstitial regions less significant.

A proposed model which may be more realistic is to consider an equal number $S = +^1/_2$ and $S = -^1/_2$ disclinations to be randomly distributed in space. The director lines interconnecting these are then drawn so as to minimize the curvature. The scattering pattern associated with such a model is believed to qualitatively correspond to that associated with the simpler models just decribed. Such models lead to a scattered intensity maximum occurring at a θ_{max} related to the average spacing of the disclinations.

Annealing is believed to be associated with diffusion coalescence of $S = +^1/_2$ and $-^1/_2$ disclinations leading to their annihilation.[5] This results in a decrease in the remaining number which rearrange themselves randomly in space, with a larger average distance between them and hence a smaller θ_{max} as is observed.

The diffusion coalescence and annihilation of disclinations is believed to be driven by the decrease in free energy associated with a lowering of the disclination density.[5] As previously indicated, the energy associated with disclinations is related to the elastic force constants associated with the bending of the lines designating the director orientation. The curvature and hence the energy decreases with decreasing density of disclinations.

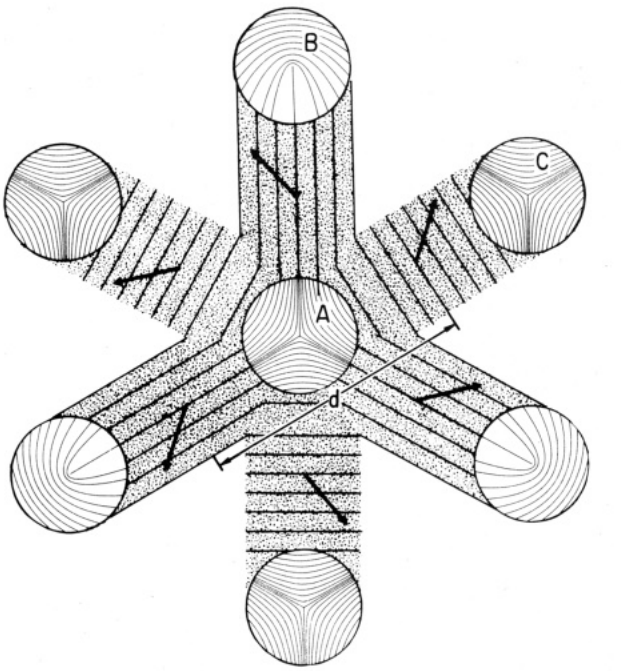

Figure 12. Schematical illustration showing an example of many-body models composed of the disclinations of $S = \pm^1/_2$.

Acknowledgment. The Kyoto group thanks the Japanese Ministry of International Trade and Industry (MITI) and Polyplastics Co. LTD., Japan, for partial support of this work. The Amherst group appreciates the support of the Materials Research Laboratory of the University of Massachusetts and the Division of Materials Research of the National Science Foundation.

Registry No. (*p*-Phenylsulfonylhydroquinone)(1,10-bis(4′-chloroformylphenoxy)decane) (copolymer), 116665-00-0; (*p*-phenylsulfonylhydroquinone)(1,10-bis(4′-chloroformylphenoxy)decane) (SRU), 102961-46-6; (1,4-benzenedicarboxylic acid)(1,2-ethanediol)(4-hydroxybenzoic acid) (copolymer), 25822-54-2.

References and Notes

(1) Oseen, C. W. *Trans. Faraday Soc.* **1933**, *29*, 883.
(2) Frank, F. C. *Discuss Faraday Soc.* **1958**, *25*, 19.
(3) Jackson, W. J.; Kuhfuss, H. F. *J. Polym. Sci., Polym. Chem. Ed.* **1976**, *14*, 2043.
(4) Furukawa, A.; Lenz, R. W. *Makromol. Chem., Macromol. Symp.* **1986**, *2*, 3.
(5) Nakai, A.; Shiwaku, T.; Hasegawa, H.; Hashimoto, T. *Macromolecules* **1986**, *19*, 3010.
(6) Shiwaku, T.; Nakai, A.; Hasegawa, H.; Hashimoto, T. *Polym. Commun.* **1987**, *28*, 174.
(7) Clough, S.; van Aartsen, J. J.; Stein, R. S. *J. Appl. Phys.* **1965**, *36*, 3072.
(8) Stein, R. S.; Erhardt, P. E.; van Aartsen, J. J.; Clough, S. B.; Rhode, M. B. *J. Polym. Sci., Part C* **1966**, *1*, 13.
(9) Moritani, M.; Hayashi, N.; Utsuo, A.; Kawai, H. *Polym. J.* **1971**, *2*, 74.
(10) Matsuo, M.; Nomura, S.; Hashimoto, T.; Kawai, H. *Polym. J.* **1974**, *6*, 151.
(11) Hasimoto, T.; Murakami, Y.; Kawai, H. *J. Polym. Sci., Polym. Phys. Ed.* **1975**, *13*, 1613.
(12) Hasimoto, T.; Ebisu, S.; Kawai, H. *J. polym. Sci., Polym. Phys. Ed.* **1981**, *19*, 59.

Conversion Chemical Heterogeneity of Graft Copolymers Prepared from Macromonomers

Jaroslav Stejskal* and Pavel Kratochvíl

Institute of Macromolecular Chemistry, Czechoslovak Academy of Sciences, 162 06 Prague 6, Czechoslovakia. *Received February 5, 1988*

ABSTRACT: The conversion chemical heterogeneity of graft copolymers prepared by statistical copolymerization of an ordinary monomer with a macromonomer has been estimated. Its extent does not depend on the molecular weight of the macromonomer. Consequently, it is comparable with that of common statistical copolymers prepared from two low molecular weight comonomers. The chemical composition distribution is broader the more the monomer reactivity ratio of the ordinary monomer differs from unity.

Introduction

Statistical copolymerization of an ordinary low molecular weight monomer with a macromonomer is an up-to-date and efficient way of preparing graft copolymers.[1] In copolymerizations comprising a macromonomer, two mechanisms producing chemical heterogeneity of products are to be considered, similar to the copolymerization of two ordinary monomers.

The statistical nature of copolymer chain formation gives rise to statistical chemical heterogeneity.[2] With macromonomers, this type of heterogeneity would be significant in typical cases.[3] The conversion heterogeneity originates due to the drift of the monomer–mixture composition (and thus also of the composition of the copolymer molecules formed) depending on the conversion of monomers into copolymer,[4] because both monomers are usually not consumed at equal rates. For a copolymerization including a macromonomer, this effect has been observed experimentally by Niwa et al.[5] and by Tsukahara et al.[6] Both types of chemical heterogeneity occur simultaneously and are superimposed[7] in any practical experiment.

The aim of this contribution is to estimate the extent of chemical heterogeneity due to the conversion in graft copolymers prepared by statistical copolymerization of an ordinary monomer with a macromonomer.

Theory

Chemical Composition Distribution (CCD). A typical feature of a statistical copolymerization which includes a macromonomer as one of the monomers is the low molar content of the macromonomer in the reaction mixture. If we denote the molar concentration of the ordinary monomer in the mixture as [A], and that of a macromonomer [M], then for [A] ≫ [M] the classical copolymerization equation reduces,[1] for the monomer reactivity ratios not too different from unity, to

$$\frac{d[A]}{d[M]} = r_A\frac{[A]}{[M]} \tag{1}$$

The chemical composition of the copolymer is thus controlled, apart from the concentration of monomers, only by the monomer reactivity ratio r_A of the low molecular weight monomer. This parameter is assumed to be, similar to the classical copolymerization of two comonomers, independent of conversion. Integration of eq 1 yields

$$\frac{[A]}{[A]_0} = \left(\frac{[M]}{[M]_0}\right)^{r_A} \tag{2}$$

The subscript 0 denotes the value of a quantity in the starting mixture, i.e., at zero conversion.

The relation between the composition of the monomer mixture, f, in terms of the mole fraction of monomer A

$$f = \frac{[A]}{[A] + [M]} \tag{3}$$

and the mole conversion of monomers to copolymer, ψ_m

$$\psi_m = 1 - \frac{[A] + [M]}{[A]_0 + [M]_0} \tag{4}$$

is obtained

$$\psi_m = 1 - \left(\frac{f}{f_0}\right)^{-(\beta+1)}\left(\frac{1-f}{1-f_0}\right)^{\beta} \tag{5}$$

after rearrangement of eq 2. The parameter β is defined as $\beta = r_A/(1 - r_A)$.

0024-9297/89/2222-0429$01.50/0